

On the Operation of Squirrel Cage Induction Motors: Damping of Converter-Generated Current Harmonics*

¹E. Normanyo and ¹J. P. Nkansah
¹University of Mines and Technology, Tarkwa, Ghana

Normanyo, E. and Nkansah, J. P. (2019), "On the Operation of Squirrel Cage Induction Motors: Damping of Converter-Generated Current Harmonics", *Ghana Journal of Technology*, Vol. 6, No. 1, pp. 18-25.

Abstract

AC to AC power electronic converters are deployed in power supply systems to regulate the stator voltage of squirrel cage induction motors in order to control the rotational speed. These converters however, are sources of current harmonics that give rise to voltage harmonics distortions. In this research, a shunt active power filter was deployed to mitigate the effects of the fifth and seventh harmonics generated by the converter which adversely modulate the ideal characteristics of the motor rotational speed, electromagnetic torque and stator current in terms of amplitude and frequency. Simulation results evidenced from speed, torque and stator current waveforms, and also from harmonic spectra show the desirability of use of shunt active power filter in mitigating power electronics converter-generated current harmonics suffered by squirrel cage induction motors.

Keywords: Converter, Current Harmonics, MATLAB/Simulink, Squirrel Cage Induction Motor, Simulation

1 Introduction

A reliable way to regulate the stator voltage of the Squirrel Cage Induction Motor (SCIM) and thereby, control its rotational speed is to deploy an AC to AC Power Electronic Converter (PEC) in the power supply circuit. About 85% of modern industries are equipped with SCIMs due to their very useful characteristics such as low cost, low maintenance, reasonable small size and good efficiency (Karmakar *et al.*, 2016; Rangel-Magdaleno *et al.*, 2016). The PEC connected to the AC mains serves as a phase-controlled AC regulator that capably converts a constant AC voltage into a variable AC voltage. This conversion assures of very high efficiency of conversion due to very low losses in the deployed Silicon Controlled Rectifiers (SCRs) of PEC. The obtained variable voltage applied at the stator input of SCIM is useful in the sense that the electromagnetic torque developed by the SCIM is proportional to the square of the stator applied voltage (Rashid, 2014). The rotational speed of SCIM is inversely proportional to the electromagnetic torque and directly proportional to the stator applied voltage (Ali *et al.*, 2018). Hence, the speed and torque of SCIM can be varied using PEC.

The drawback in using the PEC however, is its notable generation of current harmonics as it functions as a SCIM speed controller due to intermittent firing and conduction of the SCRs (Ali *et al.*, 2018). According to Donolo *et al.* (2016), irregularities due to harmonics do alter the stable spectra of SCIM characteristics. Both voltage and current harmonics are synonymous with deployed in service SCIMs. Notwithstanding, the voltage harmonics are normally generated as a result of the

prevalence of current harmonics (Jaisiva *et al.*, 2016).

According to Zhou and Shen (2017), current harmonics is exhibited by both open and closed rotor slot induction motors. Kindl *et al.* (2020) reviewed time and space harmonics in multi – phase induction machines and concluded that increased number of phases of machine decreases torque harmonics. Indeed, current harmonics phenomena in electrical machines related installations have been well acknowledged. Kastawan (2018) analysed load current harmonics effects on vertical and horizontal vibrations of a 3 – phase generator and concluded that the level of the vibration is proportional to the level of load current harmonics. Wang *et al.* (2020) deployed a carrier phase shift method in eliminating high frequency phase current harmonics in a quadruple multi 3 – phase machine drive system to achieve reduction of flux linkage harmonics, torque ripple, vibration and noise. Sumega *et al.* (2020) designed a current harmonics controller to reduce cogging torque – caused acoustic noise, vibrations, torque ripple and speed ripple in low – cost Permanent Magnet (PM) motors under flux oriented control operations to achieve improved performance of electric drive.

In a number of reported researches, attempts were made to suppress current harmonics. Alhamrouni *et al.* (2020) compensated harmonic currents and reactive power using designed passive and active shunt hybrid power filters that involved several control systems of p – q theory and Proportional – Integral (PI) controller for high – power nonlinear loads. Jafrodi *et al.* (2020) combined passive and active power filters in series based on Sliding Mode Control (SMC) technique to compensate the current harmonics. Srinivas *et al.* (2020) used shunt Active

*Manuscript received June 27, 2021

Revised version accepted September 22, 2021

Power Filter (APF) and Artificial Neural Network (ANN) controller to reduce source side current harmonics in a power system to achieve high system stability. Wu *et al.* (2020) suppressed current harmonics of asymmetric dual 3 – phase Permanent Magnet Synchronous Motor (PMSM) using a feedforward voltage compensation technique. Kastawan *et al.* (2020) used phase shifting transformers to reduce source current harmonics generated by variable speed drives of a stenter blower machine of a textile industry. Yuan *et al.* (2015) reduced undesired 5th and 7th stator harmonic currents in a 6–phase PMSM supplied by two independent voltage source inverters using an improved vector control algorithm based on vector space decomposition transformation method. Sujith and Parma (2019) developed an adaptive linear neural network for the estimation of harmonics using an APF whilst Imam *et al.* (2020) gave a detailed systematic approach to the design of a shunt APF for mitigation of current and voltage harmonics to meet power quality requirements of the utility grid. In these situations, the SCIM was not considered.

For a two-level inverter-fed SCIM drive platform, Zhang *et al.* (2015) utilised Model Predictive Torque Control (MPTC) over the conventional Direct Torque Control (DTC) of SCIM drive to achieve a better damped response of torque ripple and current harmonics. Sivakumar and Muthu Selvan (2018) reduced SCIM source side current harmonics using PI – based and ANN – based shunt APF at the source end of system. Xie *et al.* (2019) solved the problem of current harmonics–caused torque ripple of SCIMs in electric vehicle drive systems using a novel control method in the feedback path based on hybrid digital morphological filters added onto the current loop to suppress the current harmonic components. Hsu (2019) made use of Fractional Order Proportional-Integral-Derivative (FOPID) controller to reduce harmonic current, motor vibration and noise on SCIMs to achieve stabilised operation of motor. Musak *et al.* (2015) suppressed low-order current harmonics in AC motor drives using a control algorithm.

Studies on damping of current harmonics of SCIM are focused mainly on attenuation of torque ripple, vibration and noise by utilising control system techniques that usually deploy PID-based or Artificial Intelligence (AI) controllers. These control systems heighten complexity by compromising system simplicity and reliability. This paper is dedicated to studies on speed and torque anomalies of SCIM caused by current harmonics generated by PEC. More importantly, mitigation of current harmonics effects on speed and torque of SCIM using an integrated shunt APF serves as the contribution of this paper. The rest of the paper is therefore structured as follows: Section

2 expounds on the mathematical modelling and computer simulations of the proposed system. Section 3 gives the simulation results and aptly discusses them. Section 4 concludes on the research outcome.

2 Resources and Methods Used

2.1 Mathematical Modelling

Fig. 1 (modified after Sebasthirani and Porkumar, 2014) gives the concept of damping of the current harmonics using the shunt APF.

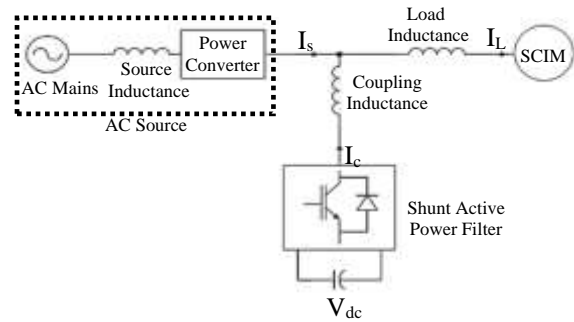


Fig. 1 Conceptual Diagram of the Damping of Current Harmonics-Induced Vibrations of SCIM

2.1.1 Modelling of the Squirrel Cage Induction Motor

The dynamic model of the stator of the SCIM is represented in its natural coordinates (a, b and c) by Equations (1), (2) and (3) (Korondi *et al.*, 2014).

$$U_{sa} = i_{sa} \cdot R_{sa} + \frac{d\Psi_{sa}}{dt} \quad (1)$$

$$U_{sb} = i_{sb} \cdot R_{sb} + \frac{d\Psi_{sb}}{dt} \quad (2)$$

$$U_{sc} = i_{sc} \cdot R_{sc} + \frac{d\Psi_{sc}}{dt} \quad (3)$$

where, U_{sa} , U_{sb} and U_{sc} are stator voltages of phases a, b and c, respectively in volts (V), i_{sa} , i_{sb} and i_{sc} are stator currents of phases a, b and c, respectively in amps (A), $R_{sa} = R_{sb} = R_{sc}$ are stator resistances of phases a, b and c, respectively in ohms (Ω), Ψ_{sa} , Ψ_{sb} and Ψ_{sc} are total stator fluxes of the phases a, b and c, respectively in Weber (Wb).

A vector representation of the dynamic model of the SCIM stator is presented in Equation (4). Likewise, the model of the rotor along its natural coordinates is presented as a vector using Equation (5) (Korondi *et al.*, 2014).

$$\vec{U}_s = \vec{i}_s \cdot R_s + \frac{d\vec{\Psi}_s}{dt} \quad (4)$$

$$\vec{U}_r = \vec{i}_r \cdot R_r + \frac{d\vec{\Psi}_r}{dt} \quad (5)$$

where, \vec{U}_s and \vec{U}_r are stator and rotor vector voltages, respectively in volts (V), \vec{i}_s and \vec{i}_r are current vectors of stator and rotor, respectively in amps (A), R_s and R_r are stator and rotor resistances, respectively in ohms (Ω), $\vec{\Psi}_s$ and $\vec{\Psi}_r$ are stator and rotor flux vectors, respectively in Weber (Wb). Korondi *et al.* (2014) expresses the flux vector of the stator and rotor, in Equations (6) and (7), in their natural coordinate system. Hence, the Equation (4), (5), (6) and (7) all together represent the general SCIM equations:

$$\vec{\Psi}_s = \vec{i}_s \cdot L_s + \vec{i}_r \cdot e^{j\alpha} \cdot L_m \quad (6)$$

$$\vec{\Psi}_r = \vec{i}_r \cdot L_r + \vec{i}_s \cdot e^{-j\alpha} \cdot L_m \quad (7)$$

where, L_s is three-phase resultant inductance of the stator in henry (H), L_r is three-phase resultant inductance of the rotor in henry (H), L_m is three-phase mutual inductance in henry (H). Considering $\vec{\Psi}_r$ and \vec{i}_s as state variables, Equation (8) is a state space model developed from the dynamic model of the SCIM in the d-q (direct quadrature) coordinate system (Korondi *et al.*, 2014). The usefulness of these equations are realised when modelling the SCIM in MATLAB/Simulink software (Bellure and Aspalli, 2015).

$$\frac{d}{dt} \begin{bmatrix} i_{sd} \\ i_{sq} \\ \Psi_{rd} \\ \Psi_{rq} \end{bmatrix} = \begin{bmatrix} -\frac{\bar{R}}{L_s \sigma} & 0 & \frac{L_m R_r}{L_s \sigma L_r^2} & \frac{L_m \omega_r}{L_s \sigma L_r} \\ 0 & -\frac{\bar{R}}{L_s \sigma} & -\frac{L_m \omega_r}{L_s \sigma L_r} & \frac{L_m R_r}{L_s \sigma L_r^2} \\ \frac{L_m R_r}{L_r} & 0 & -\frac{R_r}{L_r} & -\omega_r \\ 0 & \frac{L_m R_r}{L_r} & \omega_r & -\frac{R_r}{L_r} \end{bmatrix} \begin{bmatrix} i_{sd} \\ i_{sq} \\ \Psi_{rd} \\ \Psi_{rq} \end{bmatrix} + \begin{bmatrix} \frac{1}{L_s \sigma} & 0 \\ 0 & \frac{1}{L_s \sigma} \\ 0 & 0 \\ 0 & 0 \end{bmatrix} \begin{bmatrix} u_{sd} \\ u_{sq} \end{bmatrix} \quad (8)$$

where, i_{sd} and i_{sq} are stator currents of the d-q axis (A), Ψ_{rd} and Ψ_{rq} are rotor fluxes of the d-q axis (Wb), \bar{R} is rotor resistance vector (Ω), $\sigma = 1 - \frac{L_m^2}{L_s \times L_r}$ is total leakage coefficient and u_{sd} and u_{sq} are stator voltages of the d-q axis (V).

2.1.2 Modelling of the AC Power Source

The AC source comprises the stiff power source, the source impedance and the power converter. In modelling the AC power source, the AC mains output phase voltages are given by Equations (9) to (14).

$$V_{sa} = V_a - (i_{sa} R_{sa}) - L_{sa} (di_{sa}/dt) \quad (9)$$

$$V_{sb} = V_b - (i_{sb} R_{sb}) - L_{sb} (di_{sb}/dt) \quad (10)$$

$$V_{sc} = V_c - (i_{sc} R_{sc}) - L_{sc} (di_{sc}/dt) \quad (11)$$

$$V_a = V_s \sin(\omega t + \phi) \quad (12)$$

$$V_b = V_s \sin\left(\omega t + \phi - \frac{2\pi}{3}\right) \quad (13)$$

$$V_c = V_s \sin\left(\omega t + \phi + \frac{2\pi}{3}\right) \quad (14)$$

where, V_{sa} , V_{sb} , V_{sc} are output phase voltages of AC mains in volts, V_a , V_b , V_c are phase vectors of the mains voltage in volts without consideration of the source impedance, i_{sa} , i_{sb} , i_{sc} are mains phase currents in amperes, L_{sa} , L_{sb} , L_{sc} are mains source inductances in henry, i_{sa} , i_{sb} , i_{sc} are mains phase currents in amperes, V_s is mains line voltage in volts, ω is angular frequency of the waveform in radian/sec, ϕ is phase difference (angle) in radian. The source impedance is expressed as in Equation (15).

$$Z_s = R_s + jX_s \quad (15)$$

where, Z_s is source impedance in ohms, R_s is source resistance in ohms, X_s is source reactance in ohms.

The PEC consists of ten (10) SCRs as shown in Fig. 2. It supplies varying voltage to the stator terminals and actualising working modes of SCIM in all the four quadrants of operation by way of regulating the triggering delay and conduction angles of its SCRs.

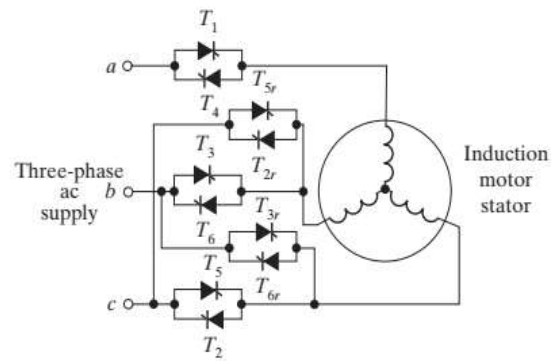


Fig. 2 Topology of the Power Electronic Converter Connected to the Stator Winding of Induction Motor

The relevant governing equations of the PEC are expressed by Equations (16), (17) and (18) (Rashid, 2014).

$$v_o(t) = v_m \sin(\omega t + \alpha) \quad (16)$$

$$i_{as}(t) = \frac{V_m}{Z_{im}} \left[\sin(\omega_s t + \alpha - \theta) - \sin \alpha - \theta e^{\frac{-\omega t}{\tan \theta}} \right] \quad (17)$$

$$\sin(\beta + \alpha - \theta) - \sin \alpha - \theta \frac{-\beta}{e^{\tan \theta}} \quad (18)$$

where, $v_o(t)$ is output voltage of PEC which is applied to the stator of SCIM for a triggering delay angle, α of the conducting SCRs, v_m is peak stator voltage of SCIM, ω is AC mains supply frequency, α is the triggering delay angle of SCRs, $i_{as}(t)$ is the corresponding instantaneous output current of PEC applied to the stator phases of SCIM for the interval $0 \leq \omega t \leq \beta$, Z_{im} is the equivalent impedance of SCIM, ω_s is synchronous speed of SCIM, θ is power factor angle of SCIM and β is conduction angle of the SCRs obtained when the current, $i_{as}(t)$ becomes zero.

2.1.3 Modelling of the Shunt Active Power Filter

The shunt APF is utilised in this research to deal with the PEC-generated current harmonics in the course of operation of SCIM. It offers desirable bandwidth of operation, adaptation and elimination of resonance. The shunt APF has the characteristic of subtracting harmonic current from a power system (Sebasthirani and Porkumaran, 2014). The Equations (19) to (27) are employed in the modelling of the shunt APF.

$$i_{ns}(t) = i_{hL}(t) - i_{hc}(t) \quad (19)$$

$$i_{hL}(t) = \sum_{n=1}^{\infty} \frac{I_m}{m} \sin(m\omega t + \phi_m) \quad (20)$$

$$i_{nL}(t) = i_{hs}(t) - i_{hc}(t) \quad (21)$$

$$i_{hs}(t) = i_{nL}(t) - (-i_{hc}(t)) \quad (22)$$

$$\begin{bmatrix} V_\alpha \\ V_\beta \\ V_0 \end{bmatrix} = \sqrt{\frac{2}{3}} \begin{bmatrix} 1 & -1/2 & -1/2 \\ 0 & \sqrt{3}/2 & -\sqrt{3}/2 \\ 1/\sqrt{2} & 1/\sqrt{2} & 1/\sqrt{2} \end{bmatrix} \begin{bmatrix} V_a \\ V_b \\ V_c \end{bmatrix} \quad (23)$$

$$\begin{bmatrix} I_\alpha \\ I_\beta \\ I_0 \end{bmatrix} = \sqrt{\frac{2}{3}} \begin{bmatrix} 1 & -1/2 & -1/2 \\ 0 & \sqrt{3}/2 & -\sqrt{3}/2 \\ 1/\sqrt{2} & 1/\sqrt{2} & 1/\sqrt{2} \end{bmatrix} \begin{bmatrix} I_a \\ I_b \\ I_c \end{bmatrix} \quad (24)$$

$$\begin{bmatrix} p = \bar{p} + \tilde{p} \\ q = \bar{q} + \tilde{q} \end{bmatrix} = \begin{bmatrix} V_\alpha & V_\beta \\ -V_\beta & V_\alpha \end{bmatrix} \begin{bmatrix} I_\alpha \\ I_\beta \end{bmatrix} \quad (25)$$

$$\begin{bmatrix} I_\alpha \\ I_\beta \end{bmatrix} = \frac{1}{V_\alpha^2 + V_\beta^2} \begin{bmatrix} V_\alpha & V_\beta \\ V_\beta & -V_\alpha \end{bmatrix} \begin{bmatrix} \tilde{p} \\ \tilde{q} \end{bmatrix} \quad (26)$$

$$\begin{bmatrix} I_a^* \\ I_b^* \\ I_c^* \end{bmatrix} = \sqrt{\frac{2}{3}} \begin{bmatrix} 1 & 0 \\ -1/2 & \sqrt{3}/2 \\ -1/2 & -\sqrt{3}/2 \end{bmatrix} \begin{bmatrix} I_\alpha \\ I_\beta \end{bmatrix} \quad (27)$$

where, $i_{nL}(t)$ is non-harmonic source current (A),

$i_{hL}(t)$ and $i_{hc}(t)$ are harmonic load and compensating currents, respectively (A), I_m is peak load current (A), m is $2n - 1$ is harmonic order, ω is angular frequency (rad/s), ϕ_m is phase difference of harmonic order m ($^\circ$), $i_{nL}(t)$ is non-harmonic load current (A), $i_{hs}(t)$ is harmonic source current (A), V_α, V_β and V_0 are instantaneous voltage values of the $\alpha - \beta - 0$ axes, respectively (V), V_a, V_b and V_c are instantaneous voltage values of the a-b-c axes, respectively (V), I_α, I_β and I_0 are instantaneous current values of the $\alpha - \beta - 0$ axes, respectively (A), I_a, I_b and I_c are instantaneous current values of the a-b-c axes, respectively (A), p is active power (W), \bar{p} and \tilde{p} are average and harmonic parts of the active power, respectively (W), q is reactive power (var), \bar{q} and \tilde{q} are average and harmonic parts of the reactive power, respectively (var), I_a^*, I_b^* and I_c^* are compensating current and reference of the a-b-c axes respectively (A).

2.2 Computer Simulations

The simulations investigated the time and/or frequency-based responses of the system for conditions under desired baseline characteristics of the AC mains and SCIM and also for current harmonics source to the SCIM with and without shunt APF. The SCIM speed, electromagnetic torque and mechanical load torque are related in Equation (28) and Equation (29) (Bellure and Aspulli, 2015).

$$T_e = T_L + \frac{2}{n} J \frac{d\omega_r}{dt} \quad (28)$$

$$N_r = \omega_r \times \frac{30}{\pi} \quad (29)$$

where, T_e and T_L are electromagnetic and mechanical load torques, respectively (Nm), n is number of poles of SCIM, ω_r and N_r are rotor angular speed (rad/s) and SCIM speed in (rpm), J is rotor inertia (kgm^2).

Table 1 presents the parameters and their respective values used in the modelling of SCIM using the Asynchronous Machine SI Units block in MATLAB/Simulink software. In this paper, the 5th and 7th harmonics were considered due to their frequency of occurrence in electric power systems (Donolo *et al.*, 2016). The 5th and 7th harmonics were modelled as negative and positive sequences, respectively. However, taking cognisance of the

fundamental current, the ratio of the 7th to the 5th harmonic current approximately amounts to 0.7, hence, the magnitude of the 7th harmonic is modelled to be 0.7 times that of the 5th harmonic. For the case of simulation of current harmonics condition with an integrated shunt APF, the values of parameters used are presented in Table 2. Fig. 3 is the Simulink model of the SCIM under current harmonics supply with the integrated shunt APF.

Major blocks within the shunt APF system are reference current generation module (Fig. 4), power loss compensation module (Fig. 5) and three-phase inverter (Fig. 6). The Fast Fourier transformation module is represented in Simulink software as shown in Fig. 7. The transfer function of the low-pass filter, $H(z)$ of the reference current generation module is given by Equation (30) in Z-transform (Ahmet, 2017).

$$H(z) = \frac{2.613e-06 + 1.032e-05z^{-1} + 2.548e-06z^{-2}}{1 - 2.950z^{-1} + 2.901z^{-2} - 0.951z^{-3}} \quad (30)$$

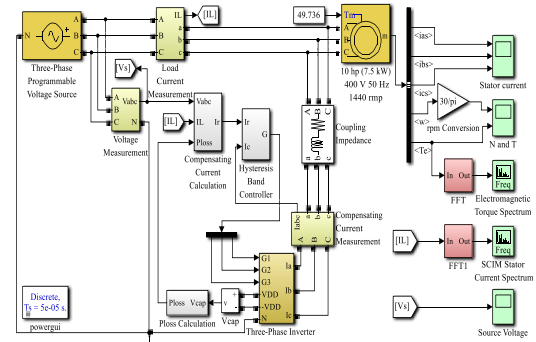


Fig. 3 Simulink Model of the Squirrel-Cage Induction Motor under 5th and 7th Current Harmonics Supply with the Integrated Shunt Active Power Filter

Table 1 Model Parameters of Squirrel-Cage Induction Motor

SN	Parameter	Value
1.	Power (kW)	7.5
2.	RMS Voltage (V)	400
3.	Peak Voltage (V)	326.599
4.	Frequency (Hz)	50
5.	Rotor Speed (rpm)	1440
6.	Stator Resistance (Ω)	0.7384
7.	Stator Inductance (H)	0.003045
8.	Rotor Resistance (Ω)	0.7402
9.	Rotor Inductance (H)	0.003045
10.	Mutual Inductance (H)	0.1241
11.	Pole Pairs	2
12.	Input Mechanical Load Torque (Nm)	49.736

(Source: Anon., 2019)

Table 2 Integrated Shunt Active Power Filter Parameters used in the Simulation of Harmonics Condition

SN	Parameter	Value
1.	Coupling Resistance (Ω)	0.0001
2.	Coupling Inductance (H)	0.0003
3.	Relay Switch-On Point	0.01
4.	Relay Switch-Off Point	-0.01
5.	Pair of Inverter Capacitors (μ F)	4700
6.	Inverter Capacitor Voltage (V)	200
7.	Reference Voltage (V)	400
8.	Output Buffer Size	650
9.	ZOH Sampling Time (s)	0.001
10.	K_p	25
11.	K_i	17
12.	Mechanical Load Torque (Nm)	49.736

(Source: Anon., 2019; Budhrani et al., 2018)

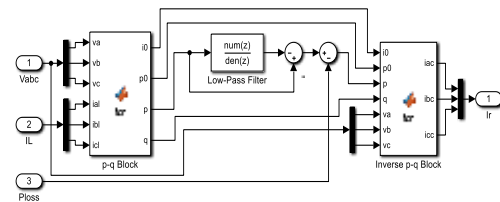


Fig. 4 Simulink Model for Generating Compensating Reference Current

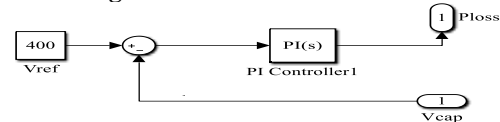


Fig. 5 Simulink Model of the Power Loss Compensation

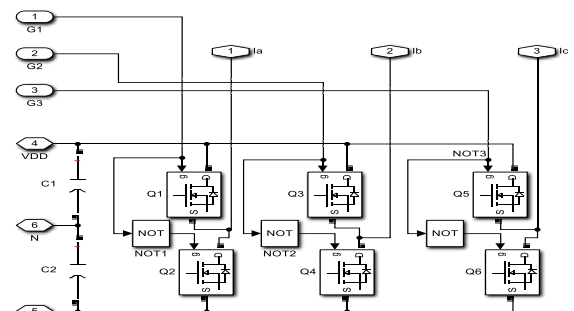


Fig. 6 Simulink Model of the Three-Phase Inverter

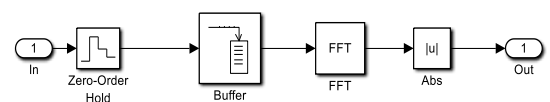


Fig. 7 Simulink Model of Fast Fourier Transformation

3 Results and Discussion

3.1 Simulation Results

3.1.1 Baseline Characteristics under Normal Squirrel-Cage Induction Motor Operations

Fig. 8 represents the waveforms of the SCIM speed and electromagnetic torque under 400 V supply, with coupled mechanical load, at a speed of 1440 rpm and without influence of current harmonics. When a load torque of 49.736 Nm was coupled to the SCIM, its electromagnetic torque approached 49.736 Nm at steady state. Fig. 9 gives the frequency spectra of the SCIM torque and stator current without current harmonics effects.

3.1.3 Characteristics under 5th and 7th Harmonics Effects and Damping Technique

The mechanical load torque coupled to the SCIM was 49.736 Nm. The 5th and 7th harmonics were superimposed on the supply to result in the waveforms and spectra. Due to the frequency specific nature of current harmonics, the frequency spectrum of the response of supply and SCIM torque are shown in Fig. 10. Fig. 11 is the waveform of the stator current to the SCIM under 5th and 7th current harmonics distortions. Fig. 12 gives the response of the speed and electromagnetic torque of the SCIM under 5th and 7th harmonics distortions without the shunt APF. Fig. 13 shows the frequency spectrum of the electromagnetic torque and stator current of the SCIM under 5th and 7th harmonics condition after integrating with the shunt APF.

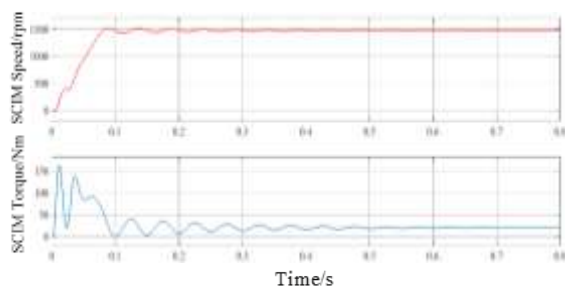


Fig. 8 Waveforms of Speed and Torque under Normal SCIM Operation

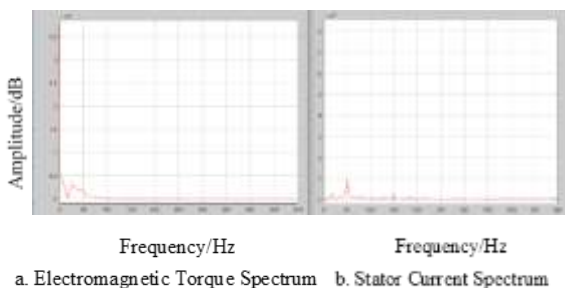


Fig. 9 Torque and Stator Current Frequency Spectra without Current Harmonics

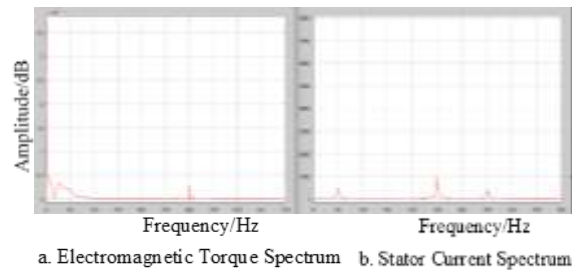


Fig. 10 Torque and Stator Current Frequency Spectra under Current Harmonics Condition

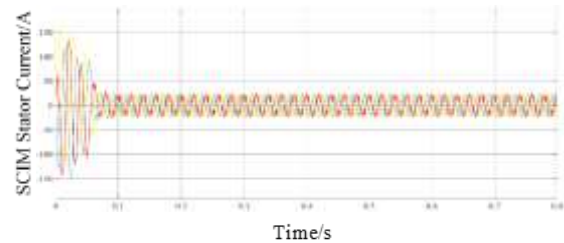


Fig. 11 5th and 7th Harmonics Distortion on Squirrel Cage Induction Motor Stator Current

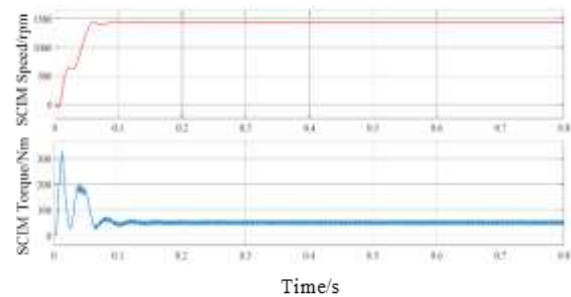


Fig. 12 Responses of Speed and Torque of SCIM to Current Harmonics Condition

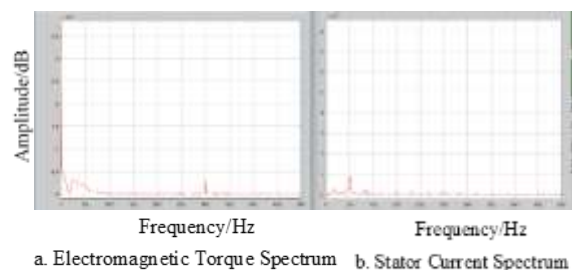


Fig. 13 Torque and Stator Current Frequency Spectra under Current Harmonics Condition with Shunt Active Power Filter

3.2 Discussion of Simulation Results

The simulation results of Fig. 8 show the baseline characteristics in terms of SCIM speed and electromagnetic torque. On start, between $t = 0 \text{ s} - 0.1 \text{ s}$, the speed rose to 1509 rpm at peak time, $t = 0.09 \text{ s}$. The torque underwent turbulent transient characteristic after maximum 162 Nm at peak time, $t = 0.012 \text{ s}$. Between $t = 0.1 \text{ s} - 0.2 \text{ s}$, the speed overshoot again to 1516 rpm however oscillating

within 1471 ± 45.6 rpm. The torque decreased from a maximum of 39.6 Nm at $t = 0.125$ s to 7 Nm at $t = 0.2$ s. Hence, the torque oscillated with values about 23.3 ± 16.31 Nm. From $t = 0.2$ s – 0.8 s, the speed and torque gradually settled to the rated values of 1440 rpm and 49.736 Nm, respectively.

The introduction of frequency analysis enabled the identification of superimposed signal constituents at their occurring frequencies with respective amplitudes of intensity. Fig. 9a is a typical characteristic of SCIM having no current harmonics sources from the power supply side of SCIM (Donolo *et al.*, 2016). The peak at 0 Hz is the mean power component. The peak value occurring at 50 Hz in Fig. 9b, is an indication of the dominant fundamental frequency component of the ideal power supply to SCIM. This includes the existing filter present, even at normal operating conditions.

The current harmonics effects of the PEC on SCIM resulted in the responses in Fig. 10. Fig. 10a gave a 300 Hz peak. This indicates an imposed rippling effect on the ideal electromagnetic torque characteristic. Fig. 10b also exhibits peaks at 250 Hz and 350 Hz. These peaks occurred at different amplitudes because, the amplitude of the 7th harmonic is 0.7 times that of the 5th harmonic. The stator current as shown in Fig. 11 was distorted in all three phases. As a result of the mechanical loading on the SCIM, the ideal steady state of the torque was to settle at 49.736 Nm. However, Fig. 12 shows an oscillation of the electromagnetic torque within 49.84 ± 9.73 Nm. The speed exhibited subtle oscillation along a path identical to its ideal characteristics in Fig. 8.

Fig. 13b showed an improved characteristic of the stator current spectrum with the integrated shunt APF, compared to the ideal spectrum in Fig. 9b. The ideal stator current spectrum showed subtle projections of frequencies; however, these frequencies together with the 5th and 7th harmonics frequencies were filtered by the shunt APF. The 300 Hz peak in the Fig. 13a remained identical to that of Fig. 10. The resulting electromagnetic torque waveform after integrating the shunt APF ranged within 49.81 ± 9.71 Nm.

4 Conclusion

Frequency analysis, speed and torque characteristics were useful for qualifying the effects of current harmonics generated by PEC on the speed and electromagnetic torque of an operating SCIM. All current harmonics components within the stator current were filtered out. The current harmonics, torque ripple at 300 Hz and voltage distortions are effects of the 5th and 7th harmonics. Use of shunt APF is a useful approach to damping the effects of PEC-generated current harmonics on SCIM.

References

- Ahmet, T. K. (2017), "Signal Processing", *Unpublished BSc Lecture Notes*, Yildiz Technical University, Istanbul, 53 pp.
- Alhamrouni, I., Hanafi, F. N. Salem, M. Rahman, N. H. A., Jusoh, A. and Sutikno, T. (2020), "Design of Shunt Hybrid Active Power Filter for Compensating Harmonic Currents and Reactive Power", *TELKOMNIKA Telecommunication, Computing, Electronics and Control*, Vol. 18, No. 4, pp. 2148-2157.
- Ali, M., Iqbal, A. and Khan, M. R. (2018), "AC - AC Converters", In Chap. 14 of *Power Electronics Handbook*, Rashid, M. R. (ed.), 4th edition, Butterworth-Heinemann, Oxford, UK, pp. 417-456.
- Anon. (2019), "Asynchronous Machine", *www.mathworks.com*. Accessed: April 6, 2019.
- Bellure, A. and Aspalli, M. S. (2015), "Dynamic d-q Model of Induction Motor Using Simulink", *International Journal of Engineering Trends and Technology*, Vol. 24, No. 5, pp. 252-257.
- Budhrani, A. H., Bhayani, K. J. and Pathak, A. R. (2018), "Design Parameters of Shunt Active Filter for Harmonics Current Mitigation", *Journal of Energy and Management*, Vol. 10, No. 2, pp. 59-65.
- Donolo, P., Bossio, G., De Angelo, C., García, G. and Donolo, M. (2016), "Voltage Unbalance and Harmonic Distortion Effects on Induction Motor Power, Torque and Vibrations", *Electric Power Systems Research*, Vol. 140, No. 3, pp. 866-873.
- Hsu, C-H. (2019), "Fractional Order PID Control for Reduction of Vibration and Noise on Induction Motor", *IEEE Transactions on Magnetics*, Vol. 55, No. 11, pp. 1-7.
- Imam, A. A., Sreerama Kumar, R. and Al-Turki, Y. A. (2020), "Modelling and Simulation of a PI Controlled Shunt Active Power Filter for Power Quality Enhancement based on P-Q Theory", *Electronics*, Vol. 9, 637, 17 pp. doi:10.3390/electronics9040637.
- Jafrodi, S. T., Ghanbari, M., Mahmoudian, M., Najafi, A., Rodrigues, E. M. G. and Pouresmaeil, E. (2020), "A Novel Control Strategy to Active Power Filter with Load Voltage Support Considering Current Harmonic Compensation", *Applied Sciences*, Vol. 10, 1664, 18 pp. doi:10.3390/app10051664.
- Jaisiva, S., Neelan, S. and Ilansezhian, T. (2016), "Harmonic Analysis in Non-linear Loads of Power System", *International Research Journal of Engineering and Technology*, Vol. 3, Issue 5, pp. 1474-1478.
- Karmakar, S., Chattopadhyay, S., Mitra, M. and Sengupta, S. (2016), "Induction Motor and Faults", in *Induction Motor Fault Diagnosis*, Springer, Singapore, 1st edition, pp. 7-28.
- Kastawan, I. M. W. (2018), "Effect of Load Current Harmonics on Vibration of Three-Phase

- Generator”, In *MATEC Web of Conferences, EDP Sciences*, Vol. 197, 6 pp. <https://doi.org/10.1051/mateconf/201819711023>. Accessed: June 14, 2021.
- Kastawan, I. M. W., Yusuf, E. and Fadhilah, A. (2020), “Simulation of Source Current Harmonic Elimination Technique using Phase Shift-ing Transformer”, In: *IOP Conf. Series: Materials Science and Engineering, IOP Publishing*, Vol. 830, No. 3, 7 pp. <https://doi.org/10.1088/1757-899X/830/3/032028>. Accessed: June 14, 2021.
- Kindl, V., Cermak, R., Ferkova, Z. and Skala, B. (2020), “Review of Time and Space Harmonics in Multi-Phase Induction Machine”, *Energies*, Vol. 13, 496, 17 pp. doi:10.3390/en13020496.
- Korondi, P., Samu, K., Raj, L., Décsei-Paróczy, A., Fodor, D., Vásárhelyi, J. and Vass, J. (2014), “Modelling Induction Motors”, in *Digital Servo Drives*, Budapest University of Technology and Economics, Budapest, 1st edition, pp. 198–214.
- Musak, M., Stulrajter, M., Hrabovcova, V., Cacciato, M., Scarcella, G. and Scelba, G. (2015), “Suppression of Low-order Current Harmonics in AC Motor Drives via Multiple Reference Frames based Control Algorithm”, *Electric Power Components and Systems*, Vol. 43, No. 18, pp. 2059–2068.
- Rangel-Magdaleno, J., Peregrina-Barreto, H., Ramirez-Cortes, J., Morales-Caporal, R. and Cruz-Vega, I. (2016), “Vibration Analysis of Partially Damaged Rotor Bar in Induction Motor under Different Load Condition Using DWT”, *Shock and Vibration*, Vol. 2016, No. 4, pp. 144–155.
- Rashid, M. R. (2014), *Power Electronics: Devices, Circuits, and Applications*, 4th edition, Pearson Education Ltd., Harlow, England. 1022 pp.
- Sebasthirani, K. and Porkumaran, K. (2014), “Performance Enhancement of Shunt Active Power Filter with Fuzzy and Hysteresis Controllers”, *Journal of Theoretical and Applied Information Technology*, Vol. 60, No. 2, pp. 284–291.
- Sivakumar, A. and Muthu Selvan, N. B. (2018), “Reduction of Source Current Harmonics in ANN Controlled Induction Motor”, *Alexandria Engineering Journal*, Vol. 57, pp. 1489–1499.
- Sujith, M. and Padma, S. (2019), “Optimisation of Harmonics with Active Power Filter Based on ADALINE Neural Network”, *Microprocessors and Microsystems*, Vol. 73, pp. 1–16. <https://doi.org/10.1016/j.micpro.2019.02.02976>. Accessed: May 22, 2020.
- Sumega, M., Rafajdus, P. and Stulrajter, M. (2020), “Current Harmonics Controller for Reduction of Acoustic Noise, Vibrations and Torque Ripple Caused by Cogging Torque in PM Motors under FOC Operation”, *Energies*, Vol. 13, 2534, 13 pp.
- Wang, X., Yan, H., Buticchi, G., Gu, C. and Zhang, H. (2020), “Equivalent Phase Current Harmonic Elimination in Quadruple Three-Phase Drives based on Carrier Phase Shift Method”, *Energies*, Vol. 13, 2709, pp. 11. doi:10.3390/en13112709.
- Wu, Z., Gu, W., Lu, K., Zhu, Y. and Guan, J. (2020), “Current Harmonic Suppression Algorithm for Asymmetric Dual Three-Phase PMSM”, *Applied Sciences*, Vol. 10, 18 pp. doi:10.3390/app10030954.
- Xie, F., Liang, K., Wu, W., Hong, W. and Qiu, C. (2019), “Multiple Harmonic Suppression Method for Induction Motor based on Hybrid Morphological Filters”, *IEEE Access*, Vol. 7, pp. 151618–151627. doi: 10.1109/ACCESS.2019.2948276.
- Yuan, L., Chen, M-L., Shen, J-Q. and Xiao, F. (2015), “Current Harmonics Elimination Control Method for Six-Phase PM Synchronous Motor Drives”, *ISA Transactions*, 7 pp., doi: <http://dx.doi.org/10.1016/j.isatra.2015.09.013>.
- Zhang, Y., Yang, H. and Xia, B. (2015), “Model Predictive Torque Control of Induction Motor Drives with Reduced Torque Ripple”, *IET Electric Power Applications*, Vol. 9, No. 9, pp. 595–604.
- Zhou, G-Y and Shen, J-X (2017), “Current Harmonics in Induction Machine with Closed-Slot Rotor”, *IEEE Transactions on Industry Applications*, Vol. 53, No. 1, pp. 134–142.

Authors



E. Normanyo is a Senior Lecturer in the Electrical and Electronic Engineering Department at the University of Mines and Technology, Tarkwa, Ghana. He holds MSc degree in Electromechanical Engineering from the Kharkov State University, Ukraine. He is a member of the Ghana Institution of Engineers. His research interests include industrial automation, industrial energy management, instrumentation systems, control engineering, automated electric drives and mechatronics.



J. P. Nkansah is a Graduate Student from the Electrical and Electronic Engineering Department at the University of Mines and Technology, Tarkwa, Ghana. His research interests include power quality, instrumentation and control, electrical machines and drives, and artificial intelligence.